Review Article
Academic Platform Journal of Natural Hazards and Disaster Management
5(2) 2024: 76-100, DOI: 10.52114/apjhad.1557231

Time Series Analysis from 1984 to 2023 of Earth Observation Satellites Data for Evaluating Changes in Vegetation Cover and Health at Flaring Sites in the Niger Delta, Nigeria

Barnabas O. Morakinyo[1*]

Department of Surveying & Geoinformatics, Faculty of Environmental Sciences, BAZE University, Abuja, Nigeria

Received: / Accepted: 27-September-2024 / 17-December-2024

Abstract

Normalized Difference Vegetation Index (NDVI) is the most popular vegetation index used to address the challenges of multi-spectral imagery, such as the evaluation of vegetation. The data (11 Landsat 5 TM, 49 Landsat 7 ETM+, 27 Landsat 8 OLI-TIRS, and 15 Landsat 9 OLI-TIRS) dated from 10/10/1984 to 17/12/2023 with < 3 % cloud cover was used to study 11 flaring sites in Rivers State, Nigeria. Data processing and analysis were carried out using MATLAB code. For Landsat 5 and 7, NDVI was determined from the atmospherically corrected multispectral bands (1-4) and for Landsat 8 and 9, bands (2-5) in the N, E, S and W directions at distances 60m, 90m, 120m and 240m from the flare. Generally, the results show that the NDVI at 60m are the lowest. NDVI increases as distance increases to 90m, 120m and 240m from the flare for all the sites. NDVI for all sites decreases as each year passes. However, Onne station shows an unsteady pattern for the years (1984-2007) before the station was built. The lowest mean NDVI (0.290) obtained from all the 11 sites is recorded at Umudioga 60m E from the flare stack, followed by Obigbo with (0.300) at 60m E from the flare. Standard deviation (SD) for each site is small with a range value (5.0786×10^{-5} - 2.0689×10^{-4}). Therefore, it can be concluded that Landsat sensors can be used to evaluate the changes in vegetation cover and health at the flaring sites in the Niger Delta.

Key words: Time series, Evaluating, Changes, Vegetation cover and health, Environmental science

1. Introduction

Flaring is a great factor contributing to the ongoing climate change in the entire world with the Niger Delta, Nigeria, not an exception. Several authors have studied the impacts of gas flaring in the environment worldwide which include increase in temperature [1, 2]; environmental pollution [1, 3, 4, 5]; contamination of vegetation [6]; destruction of vegetation and agricultural pursuits [7, 8, 9]. The negative impacts of flaring in the Niger Delta include stunted growth and/or death of farm produce, reduction and destruction of agricultural activities and vegetation [2, 3, 4, 7, 10, 11, 12, 13, 14].

Normalized Difference Vegetation Index (NDVI) is one of the primaries and the most well received vegetation index used for the vegetation assessment through remote sensing technology. The evaluation of vegetation helps in land use studies, land cover changes, commercial agriculture etc. NDVI which has a long history and simplicity can easily be obtained from any multispectral sensor with a visible and a near Infra-Red band, hence the reason for its general application [15].

[*] Corresponding Author e-mail: barnabas.ojo@bazeuniversity.edu.ng

Globally, research has shown that NDVI is successful to distinguish non-forest, sparse forest, dense forest, agricultural fields and savannah. For example, assessments of the impact of climate on vegetation dynamics over East Africa from 1982 to 2015 [16]; drought monitoring in the Hetao plain, Mongolia of Northwest China [17, 18], in North America [19], and in Turkey [20]; forest health and vegetation changes in Germany [21, 22], in China [23], and in Greece [24]. Also, for monitoring land cover dynamics of the United Kingdom [25]; ecological environmental change in China [26]; land use land cover (LULC) changes of Pakistan's Southern Punjab Province [27]; systematic planning of urban environment [28, 29]; and global vegetation monitoring [30].

Additionally, evergreen forests are determined against seasonal forest types by the NDVI [31], and vegetation properties of various kinds are also estimated by the same NDVI, including the leaf area index (LAI) [32]. Other areas of applications of NDVI include but are not limited to the study of chlorophyll concentration in leaves [33]; productivity of plants [34] and plant stress [35]. The robustness of the NDVI-related models is directly determined by the reliability of the NDVI [36].

The consistent use of NDVI among different sensors and platforms is the primary factor for the promotion of its effectiveness for the assessment of vegetation [37]. However, atmospheric effect, NDVI susceptibility to saturation, and the quality of sensor are the major difficulties facing NDVI [15]. The problem of the effects of scattered radiation in the atmosphere is reduced by using the reflectance for retrieval of NDVI [38]. NDVI values of -1 to 1 are the range of values of NDVI whether radiance, reflectance, or digital number (DN) is used as input. Water bodies give negative NDVI [3, 4], rocks, sands, or concrete surfaces give close to zero [3, 2], and vegetation, including crops, shrubs, grasses, and forests give positive NDVI values [38]. The higher values of NDVI suggest healthy vegetation [2, 3, 4].

For the past four decades NDVI products from Advanced Very High-Resolution Radiometer (AVHRR) and MODerate Resolution Imaging Spectroradiometer (MODIS) have used time-series analysis [3, 4, 7, 15]. The applications of time-series NDVI includes monitoring change in vegetation [39, 6, 40], land cover types classification [2], simulation of environmental dynamics [41], extraction of vegetation phenology [42] etc.

Many studies have been carried out on the policies regarding gas flaring globally. For example [43] found out that in Canada, the United Kingdom, Saudi Arabia, and Norway strict regulatory measures for flaring gas were put in place. It is required for oil companies to submit their environmental impact assessments on expected emissions and discharges from gas flaring; and to provide the comprehensive precautionary measures put in place for mitigating the environmental impacts of their activities [43]. Also, the advanced countries such as United States of America, Canada, United Kingdom, Norway etc. employed modern technologies for capturing flared gas for electricity generation which in turn eliminates gas flaring in the sector [43]. In Nigeria, policy coherence around gas flaring has been slowed by political partisanship, poor governance, lack of regulatory compliance, and policy conflict between environmental protection and economic development priorities [44].

In addition, in Nigeria weak enforcement of the existing anti-gas-flaring laws, and lack of efficient regulatory legal framework for gas flare management are other challenges confronting zero flare policy that leads to oil companies continuing to flare gas [45]. A policy-specific approach toward reducing natural gas flaring and improving government quality in Nigeria is not less desirable. A gas flaring price targeting natural gas companies should be more effective in mitigating gas flaring than the wider ‘carbon price’ or pollution price/tax policy [46]. Olujobi (2020) [43] concluded that low human capacity and poor funding of anti-flaring gas policies are contributing factors to continuous flaring of gas in Nigeria.

Furthermore, several studies have been carried out on the strategies for mitigating the effects of gas flaring worldwide. Firstly, the application of Carbon Capture Utilization and Storage (CCUS) technologies which enable capturing at the source, transportation, and secure storage of Carbon dioxide (CO_2) emissions from oil and gas sectors processes [47, 48]. Also, advanced drilling such as horizontal drilling which involves drilling wells parallel to the Earth's surface, allowing for the extraction of oil and gas from multiple locations using a single wellbore [49]. This technique enables companies to access hard-to-reach reserves and increase production efficiency while reducing the environmental footprint of drilling operations [49]. Horizontal drilling reduces surface disturbance and habitat fragmentation, thereby mitigating the impact on ecosystems [50, 51].

In addition, reinjection technique is another method used for curbing the impacts of gas flaring. This technique is generally employed to maintain the presence of gas for the future use and increases the efficiency of oil production in enhanced oil recovery (EOR) activities [52]. Flare utilization methods include the application of gas turbine generator (GTG), pipeline natural gas (PNG), liquefied petroleum gas (LPG), liquefied natural gas (LNG), compressed natural gas (CNG), natural gas hydrates (NGH), gas to liquid (GL) [53].

Evaluation of the changes in the vegetation cover and health at the flaring sites in the Niger Delta using NDVI data from the Earth Observation Satellites (EOS) (Landsat 5 Thematic Mapper (TM), Landsat 7 Enhanced Thematic Mapper Plus (ETM+), Landsat 8 and Landsat 9 Operational Land Imager and Thermal Infrared Sensor (OLI-TIRS)); and the time series analysis represents the knowledge gap in this research. The crucial importance of this research is that it helps to know the range of changes in the vegetation cover and health; and also, to evaluate the extent of damages that have occurred within the period at each flaring site.

There are three (3) principal research questions for this study: (1) How correctly can Landsat Earth Observation data be used to evaluate changes in vegetation cover and health over a long period at gas flaring sites in the Niger Delta? (2) What is the rate of changes in vegetation cover and health at the specific flaring site in the Niger Delta? (3) How accurately can time series analysis be used for the assessment of the changes in vegetation cover and health at the flaring sites in the Niger Delta? Hence, the examination of the ability of Landsat 5, 7, 8 and 9 sensors to evaluate the changes in vegetation cover and health at gas flaring sites in the Niger Delta is the overall aim of the study. The following are the objectives for this research: (1) Derivation of NDVI from atmospherically corrected Landsat data in the North (N), East (E), South (S), and West (W) directions at the flaring sites; (2) Classification of land surface cover (LSC) at the flaring sites; (3) Ground validation of the satellite data to improve the results; (4) Application of time series analysis for evaluating the rate of changes in vegetation cover and health.

2. Materials and Method

2.1. Study area

Eleven (11) flaring sites including two (2) refineries (Eleme 1 and Eleme 2); seven (7) flow stations (Onne, Umurolu, Alua, Rukpokwu, Obigbo, Chokocho and Umudioga); one (1)

Liquefied Natural Gas (LNG) plant (Bonny) and one (1) oil well (Sara) all from Rivers State, Niger Delta region (Figure 1) were studied for evaluation of the changes in the vegetation cover and health from 1984 to 2023 in the Niger Delta. The size of the area examined around the flare stacks with Landsat data is 12 × 12 km, in order to include sufficient data for detailed mapping of each site so that processes not related to flaring could also be resolved.

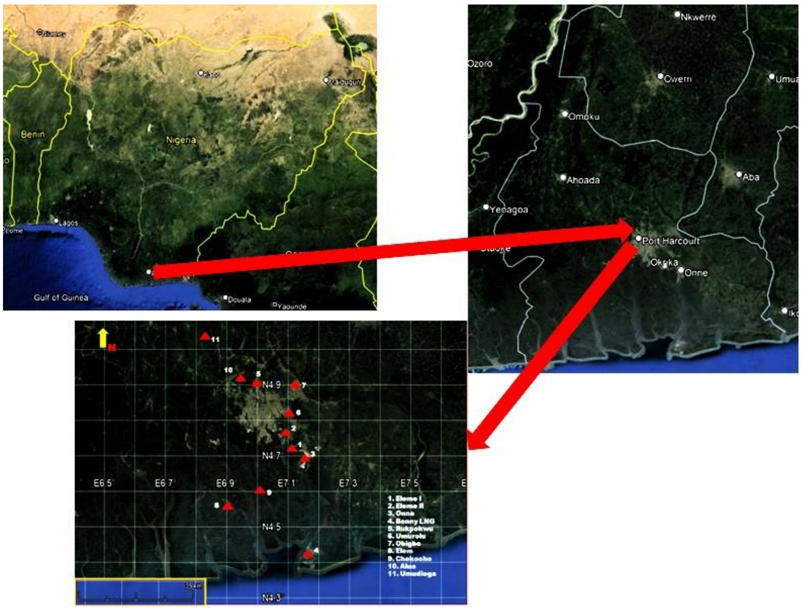

Figure 1. Top left: map of Nigeria; top right: map of Rivers State; bottom: 11 gas flaring studied sites [54].

2.2. Data used

Eleven (11) Landsat 5 TM data, forty-nine (49) Landsat 7 ETM+ data, twenty-seven (27) Landsat 8 OLI-TIRS data, and fifteen (15) Landsat 9 OLI-TIRS data dated from 10/10/1984 to 17/12/2023 with < 3 % cloud cover was used for this study. The USGS website where these data were downloaded is https://earthexplorer.usgs.gov/.

2.3. Data Analysis

2.3.1. Processing of Landsat data

1. Geo-location points were verified: Ten (10) ground control points (GCPs) were selected over the Niger Delta using Google Earth (Table 1). Twenty (20) images with five (5) images each from Landsat 5, 7**,** 8 and 9 were uploaded into the ArcGIS and the selected GCPs were identified. In Table 1, the coordinates (latitude and longitude) of the selected 10 ground control points through the Google Earth were presented in the columns 2 and 3. Columns 4 and 5 show the coordinates of the same selected 10 ground control points through Landsat 5, 7, 8 and 9 data. Column 6 provides the descriptive remarks for each of the selected points. The comparison of the coordinates of these controls obtained from the Google Earth and ArcGIS was carried out with a negligible difference found (1.0×10^{-6} to 7.3×10^{-6} m) (Table 1). This was taken as an acceptable error range for the geo-location of the imagery.

2. Removal of zero and out of range values from the data using MATLAB code, and their replacement with not a number (nan) in order to avoid divide by zero errors in calculations. Values at the upper and lower limits of the 8-bit, 12-bit and 14-bit data range which cannot be distinguished from noise were all removed.

Table 1. Geo-location point verification for Landsat 5, 7, 8 & 9 data

S/N	Google Earth Latitude (θ)	Google Earth Longitude (λ)	Landsat 5, 7, 8 & 9 Latitude (θ)	Landsat 5, 7, 8 & 9 Longitude (λ)	Remarks
1	04 24 35.42	07 09 36.00	04 24 35.40	07 09 36.00	An edge of a two storey building
2	04 25 48.34	07 11 15.41	04 25 48.34	07 11 15.39	A point on a tower
3	04 44 18.04	06 46 26.03	04 44 18.04	06 46 26.00	A two-point road junction
4	04 58 17.09	06 37 51.89	04 58 17.01	06 37 51.23	Edge of a fence.
5	04 52 59.09	06 52 09.95	04 52 59.09	06 52 09.00	A point on a LNG terminal
6	04 51 40.12	06 57 57.93	04 51 40.00	06 57 57.00	A three-point road junction
7	05 03 08.89	06 55 15.91	05 03 08.10	05 55 15.21	A three-point road junction
8	05 00 59.28	06 57 15.5	05 00 59.20	06 57 15.30	Edge of a building at Rivers International Airport
9	04 45 26.24	07 07 04.29	04 45 26.20	07 07 04.30	Edge of Eleme II fence
10	04 47 56.02	07 03 26.73	04 47 56.01	07 03 26.50	Edge of a building

3. The radiometric calibration of the multispectral bands of the data was performed. The Digital Number (DN) values were converted to the top of atmosphere (TOA) radiance values based on the sensor calibration parameters provided within the metadata files from USGS according to the Landsat 5 [55], Landsat 7 [56], Landsat 8 and Landsat 9 Science Data User's Handbooks [57] using equations 1, 2 and 3.

$$L_\lambda = G_{rescale} \times QCAL + B_{rescale} \tag{1}$$

Equation (1) is also expressed as;

$$L_\lambda = ((LMAX_\lambda - LMIN_\lambda) / (QCALMAX - QCALMIN)) \times (QCAL - QCALMIN) + LMIN_\lambda \tag{2}$$

Where:

L_λ= Spectral radiance at the sensor's aperture ($Wm^{-2}sr^{-1}\mu m^{-1}$);

$G_{rescale}$= Rescaled gain (Data product "gain" contained in the Level 1 product header or ancillary data record) ($Wm^{-2}sr^{-1}\mu m^{-1}$)/ DN;

$B_{rescale}$= Rescaled bias (Data product "offset" contained in the Level 1 product header or ancillary data record) ($Wm^{-2}sr^{-1}\mu m^{-1}$);

$QCAL$ = The quantized calibrated pixel value in DN;

$LMIN_\lambda$= The spectral radiance that is scaled to QCALMIN ($Wm^{-2}sr^{-1}\mu m^{-1}$);

$LMAX_\lambda$= The spectral radiance that is scaled to QCALMAX ($Wm^{-2}sr^{-1}\mu m^{-1}$);

$QCALMIN$ = The minimum quantized calibrated pixel value (corresponding to $LMIN_\lambda$) in DN = 1 for LPGS (a processing software version) products;

$QCALMAX$ = The maximum quantized calibrated pixel value (corresponding to $LMAX_\lambda$) in DN = 255.

For Landsat 8 and 9, the DN can be converted to spectral radiance using equation 3

$$L_\lambda = (M_L \times Q_{cal}) + A_L \text{ [57]} \tag{3}$$

Where:

L_λ= Spectral radiance ($Wm^{-2}sr^{-1}\mu m^{-1}$);

M_L= Radiance multiplicative scaling factor for the band from the metadata;

A_L= Radiance additive scaling factor for the band from the metadata;

Q_{cal} = Level 1 pixel value in DN.

4. Computation of TOA reflectance for multispectral bands 1 to 4 for Landsat 5 and 7 including the application of simple sun angle correction is done with equation (4) which assumes Lambertian surface reflectance [56, 58]:

$$\rho_P = (\pi \times L_\lambda \times d^2) / (ESUN_\lambda \times \cos\theta s) \quad (4)$$

Where:
ρ_P = Unitless effective at-satellite planetary reflectance;
L is measured per unit solid angle;
πL = Upwelling radiance over a full hemisphere;
d = Earth-Sun distance in astronomical units;
$ESUN_\lambda$= Mean solar exo-atmospheric irradiances;
θs = Solar zenith incident angle in degrees [55].

For Landsat 8 and 9, Level 1 DN of multispectral bands 2-5 can be converted to TOA uncorrected reflectance for solar elevation angle using equation 5.

$$\rho_\lambda' = (M_\rho \times Q_{cal}) + A_\rho \quad [57] \quad (5)$$

Where:
ρ_λ' = TOA Planetary Spectral Reflectance, without correction for solar angle(Unitless);
M_ρ= Reflectance multiplicative scaling factor for the band from the metadata;
A_ρ= Reflectance additive scaling factor for the band from the metadata;
Q_{cal} = Level 1 pixel value in DN.

The Landsat 8 and 9 corrected reflectance for solar elevation angle is as follows:

$$\rho_\lambda = \rho_\lambda' / \cos(\theta_{SZ}) = \rho_\lambda' / \sin(\theta_{SE}) \quad [57] \quad (6)$$

Where:
$\rho\lambda$ = TOA planetary reflectance
θ_{SZ} = Local sun elevation angle; the scene centre sun elevation angle in degrees is provided in the metadata;
θ_{SE} = Local solar zenith angle; θ_{SZ}=90°− θ_{SE}.

5. Atmospheric correction method: Dark Object Subtraction (DOS) method [59, 60] was adopted. The basic assumption is that within the image some pixels are in complete shadow and their radiances received at the satellite are due to atmospheric scattering “path radiance”. This assumption is combined with the fact that very few targets on the Earth’s surface are absolute black, so an assumed 1 % minimum reflectance is better than 0 % [61]. MODIS and Medium Resolution Imaging Spectroradiometer (MERIS) atmospheric correction algorithms [61] are based on this principle. However, this method assumes that this error is the same over the whole image.

DOS processes applied to this study mean that pixels corresponding to the darkest location (Atlantic Ocean) were selected for bands 1-4 for Landsat 5 and 7, and bands 2-5 for Landsat 8 and 9. The number of pixels obtained varies depending on the size of the darkest spot (Table 2). In Table 2, column 1 shows the image identification number of parts of Landsat 5, 7, 8 and 9 data (3 each) used for the study where the coordinates (latitude and longitude) of darkest pixels for each image for bands 1-4 for Landsat 5 and 7, and bands 2-5 for Landsat 8 and 9 were retrieved. Then, columns 2-5 presented the coordinates of darkest points for each image and for each multispectral band. The reflectance for these dark pixels was computed for each band and the minimum value obtained for each band was used as an estimate of the atmospheric reflectance for the respective band. These small errors were subtracted from the computed reflectance for each pixel of the whole image to reduce the atmospheric effects.

Table 2. Latitude and longitude of selected dark pixels over Atlantic Ocean (L5, L7, L8 & L9)

Image ID	Band 1 (Lat/Long.)	Band 2 (Lat/Long.)	Band 3 (Lat/Long.)	Band 4 (Lat/Long.)
LT51880571986017AAA04	04 20 02.07	04 20 11.21	04 21 36.79	04 21 25.05
	07 15 03.13	07 15 58.84	07 15 51.34	07 16 22.45
LT51880571987004XXX04	04 10 00.26	03 48 04.22	03 49 09.90	03 51 01.14
	07 04 43.95	07 42 00.92	07 42 01.96	07 42 23.63
LT51880571986353XXX10	04 16 48.94	04 11 40.48	04 10 16.93	04 08 08.69
	07 21 40.25	07 39 48.02	07 21 20.77	07 09 02.10
LE71880571999333AGS00	03 40 37.29	03 41 14.57	03 45 10.61	03 43 54.41
	06 35 44.23	06 35 31.92	06 34 32.91	06 32 27.08
LE71880572000352EDC00	03 57 55.38	04 17 17.76	04 18 50.68	04 19 24.42
	06 24 15.44	08 09 37.65	08 10 15.89	08 11 31.37
LE71880572003008SGS00	04 18 00.97	03 36 14.95	03 38 15.29	03 41 09.19
	07 26 14.16	07 57 22.38	07 57 45.13	07 58 49.59
	Band 2 (Lat/Long.)	Band 3 (Lat/Long.)	Band 4 (Lat/Long.)	Band 5 (Lat/Long.)
LC81880572018361LGN00	04 22 38.41	04 22 43.01	04 22 39.58	04 22 36.42
	07 04 41.30	07 04 26.11	07 04 48.01	07 04 15.20
LC81880572019364LGN00	04 16 36.71	04 18 54.00	04 17 22.05	04 16 49.02
	08 10 10.49	08 10 32.05	08 10 47.00	08 10 19.67
LC81880572021353LGN00	03 35 25.09	03 34 22.50	03 35 44.80	03 34 19.28
	07 56 24.71	07 56 12.06	07 55 31.42	07 55 37.52
LC09L1TP18805720211211	04 22 37.00	04 23 00.05	04 22 49.61	04 22 26.08
	07 04 41.13	07 04 23.05	07 04 37.01	07 04 43.59
LC09L1T18805720220317	04 06 42.08	04 06 06.59	04 06 43.39	04 04 52.90
	06 38 18.60	06 48 45.38	06 49 22.24	06 46 54.80
LC09L1T18805720231225	03 58 05.19	03 58 42.27	03 58 57.30	03 59 11.23
	06 23 32.19	06 25 23.40	06 25 41.18	06 25 59.42

6. Atmospherically corrected reflectance: This is the result obtained after the application of the DOS method in section 5 above.
7. Classification of Land Surface Cover (LSC): The atmospherically corrected reflectance bands 1-4 for Landsat 5 and 7, and bands 2-5 for Landsat 8 and 9 using the K-means function [2, 3, 4, 7, 8,10, 11, 13, 63] of the MATLAB tool were used for the first unsupervised cluster analysis for the land cover types classification. Three (3) classes of land cover (LC) types with cloud classified as the fourth class was obtained. Any of the 3 LC (Vegetation, water, soil and built up area) and the cloud as the fourth class was identified. Also, MATLAB codes were used for the elimination of the cloud class by masking. The cloud-masked reflectance was used for the second cluster analysis and 4 LC retrieved are vegetation, soil, built-up area and water [2, 6, 11, 64]. However, Landsat SWIR bands 5 and 7 (Landsat 5 and 7), and bands 6 and 7 (Landsat 8 and 9) were also employed for the classification of land cover types but they could not give useful results as the bands used, therefore, they were dropped for further analysis. Furthermore, Visual examination of Worldview-1 and 2, and IKONOS pseudo-true color images (RGB) from Google Earth and Digital Global (http://browse.digitalglobe.com/imagefinder/public.do) were also used to study and clarified the LC obtained. Results obtained from LC classification were used to summarize the LC types around each site.

8. Retrieval of NDVI in the N, E, S and W directions: The cloud-masked reflectance bands 3 and 4 for Landsat 5 and 7, and bands 4 and 5 for Landsat 8 and 9 were used for the retrieval of NDVI [3, 4]. For Landsat 5 and 7, band 3 is Red (R) and band 4 is Near Infra-Red (NIR) while for Landsat 8 and 9, band 4 is R and band 5 is NIR. The mathematical formula for NDVI is as stated in equation (7) [65].
$$NDVI = (NIR - R)/(NIR + R) \quad (7)$$
Where,
NIR = Near Infra-Red reflectance;
R = Red reflectance.

A summary of stages for the processing of Landsat 5, 7, 8 and 9 is shown in Figure 2.

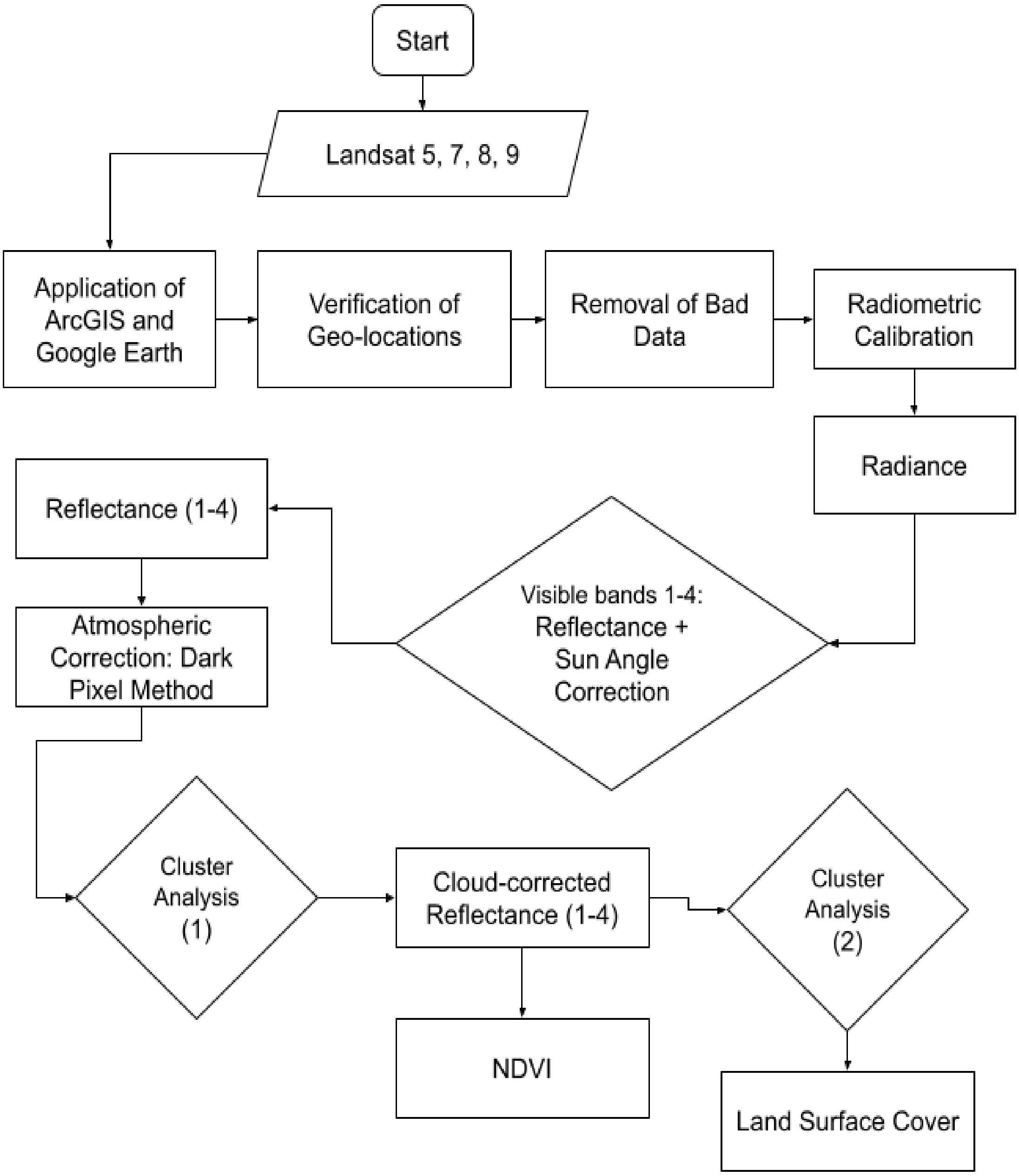

Figure 2. Methodology for processing of Landsat 5, 7, 8 and 9 data.

2.3.2. Ground validation of Landsat data

Methods and processes for the evaluation of satellite data in order to check if such data meet their stated accuracy requirements and objectives are referred to as the validation of satellite products. For this study, the validation measurements were carried out at Eleme Refineries I and II, and Onne, Alua, Chokocho and Obigbo Flow Stations on 27/07/2012 for reconnaissance activities. From 04/08/2012 to 21/09/2012[6], the first ground measurements and observations took place, which were also repeated from 05/08/2019 to 22/09/2019 [11]. The third field measurement conducted from 05/08/2023 to 22/09/2023. The in-situ data acquired are coordinates of features and points, relative humidity, air temperature, and photographs of features and locations. In addition, fieldwork activities at these 6 flaring sites confirmed that their LC (vegetation, some buildings, open land and water bodies) types are similar; and that they are the same with as other remaining flaring sites examined due to the similarity of the topography of the Niger Delta.

3. Results

3.1. Time series analysis of NDVI

Satellite data from 1984 to 2023 were used for time series analysis for this study. Generally, the results obtained presented yearly changes for all the 11 flaring sites. The NDVI values were retrieved using four cardinal points i.e., in the N, E, S and W directions at 60 m, 90 m, 120 m and 240 m from the flare stack which was at the centre of the site (0 m) 12 × 12 km. The pixels adjacent to the flare stack were used as the starting point. All Landsat data used were processed individually with NDVI for each pixel within the site retrieved. The NDVI at 60 m, 90 m, 120 m and 240 m from the flare in the N, E, S and W were retrieved for each year. Mean value for each year from the available data was computed and the range (Maximum and minimum) values of NDVI for the computed years were finally retrieved (Tables 3-6). In Table 3-6, columns 1-3 present the names of the facilities, their build time and date of available Landsat data for each site. Columns 4-7 show the mean range of NDVI values at 60 m, 90 m, 120 m and 240 m recorded for each site in the four cardinal directions.

Tables 7-17 present NDVI results at 60 m, 90 m, 120 m and 240 m from the flare in the N, E, S and W for each specific site when the entire available data for each site were processed at once. Columns 1-3 give the name of the facility for the specific site, its build date and the available Landsat data for the site in the archive. Columns 4-7 shows the NDVI results recorded in the four cardinal directions. The changes in the values of NDVI from 1984 to 2023 are presented in Figures 3-13. The results show similar trends for points between 60-120 m with a yearly reduction in the NDVI. However, at 240 m, throughout the year the NDVI results fluctuate for all the stations. Furthermore, unlike the values from 60-120 m where the highest NDVI values for all sites were recorded for the early years, the NDVI obtained for a distance of 240 m in 2023 is almost equivalent to that of the early years and even greater for some sites. For 60-120 m distance from the flare, the photosynthetic activity has been reduced to a little and/or dead with the vegetation cover and its health being negatively affected [3, 7, 11, 12, 2, 66] as shown by the results obtained. The in-situ data from ground validation activities also supported the results from the satellite data. The time of build for Eleme Refinery II, Onne Flow Station and Bonny LNG facilities are shown by a red line in the Figures 4, 5 and 7.

Table 3. Mean annual NDVI range for flaring sites at 60 m from the stack

Facility	Build time	Data dates	N (m)	E (m)	S (m)	W (m)
Eleme I	1965	1986-2023	0.20-0.69	0.36-0.75	0.54-0.84	0.23-0.78
Eleme II	1988	1984-2023	0.23-0.70	0.23-0.74	0.21-0.76	0.33-0.78
Onne	2010	1984-2023	0.48-0.82	0.51-0.79	0.48-0.82	0.51-0.79
Umurolu	Unknown	1984-2023	0.15-0.79	0.39-0.78	0.48-0.88	0.48-0.77
Bonny	1989	1986-2023	0.23-0.68	0.23-0.68	0.27-0.70	0.27-0.68
Alua	Unknown	1984-2023	0.25-0.71	0.28-0.75	0.40-0.80	0.28-0.75
Rukpokwu	Unknown	1986-2023	0.25-0.73	0.25-0.73	0.22-0.67	0.39-0.80
Obigbo	Unknown	1986-2023	0.15-0.61	0.25-0.71	0.40-0.80	0.25-0.73
Chokocho	Unknown	1986-2023	0.25-0.71	0.31-0.81	0.40-0.88	0.40-0.83
Umudioga	Unknown	1984-2023	0.40-0.74	0.46-0.76	0.23-0.78	0.18-0.78
Sara	Unknown	1986-2023	0.34-0.82	0.25-0.71	0.34-0.81	0.34-0.84

Table 4. Mean annual NDVI range for flaring sites at 90 m from the stack

Facility	Build time	Data dates	N (m)	E (m)	S (m)	W (m)
Eleme I	1965	1986-2023	0.30-0.64	0.45-0.75	0.54-0.77	0.23-0.75
Eleme II	1988	1984-2023	0.23-0.74	0.32-0.76	0.34-0.76	0.23-0.74
Onne	2010	1984-2023	0.51-0.83	0.49-0.81	0.39-0.71	0.44-0.74
Umurolu	Unknown	1984-2023	0.28-0.77	0.37-0.76	0.41-0.78	0.37-0.76
Bonny	1989	1986-2023	0.23-0.66	0.23-0.66	0.22-0.67	0.25-0.70
Alua	Unknown	1984-2023	0.26-0.74	0.22-0.74	0.19-0.72	0.38-0.84
Rukpokwu	Unknown	1986-2023	0.29-0.77	0.26-0.74	0.31-0.75	0.26-0.74
Obigbo	Unknown	1986-2023	0.31-0.75	0.26-0.74	0.23-0.74	0.21-0.74
Chokocho	Unknown	1986-2023	0.26-0.74	0.26-0.74	0.35-0.88	0.31-0.84
Umudioga	Unknown	1984-2023	0.48-0.77	0.48-0.72	0.24-0.78	0.20-0.75
Sara	Unknown	1986-2023	0.35-0.88	0.26-0.74	0.31-0.79	0.21-0.76

Table 5. Mean annual NDVI range for flaring sites at 120 m from the stack

Facility	Build time	Data dates	N (m)	E (m)	S (m)	W (m)
Eleme I	1965	1986-2023	0.49-0.72	0.55-0.82	0.41-0.62	0.50-0.72
Eleme II	1988	1984-2023	0.32-0.59	0.31-0.70	0.34-0.64	0.28-0.62
Onne	2010	1984-2023	0.32-0.62	0.39-0.64	0.35-0.59	0.34-0.70
Umurolu	Unknown	1984-2023	0.46-0.72	0.29-0.52	0.48-0.70	0.37-0.65
Bonny	1989	1986-2023	0.37-0.51	0.53-0.65	0.38-0.52	0.32-0.44
Alua	Unknown	1984-2023	0.30-0.62	0.35-0.64	0.32-0.59	0.33-0.70
Rukpokwu	Unknown	1986-2023	0.44-0.70	0.16-0.54	0.32-0.65	0.28-0.64
Obigbo	Unknown	1986-2023	0.24-0.65	0.16-0.44	0.33-0.70	0.36-0.64
Chokocho	Unknown	1986-2023	0.44-0.70	0.16-0.54	0.32-0.65	0.28-0.64
Umudioga	Unknown	1984-2023	0.48-0.70	0.16-0.42	0.32-0.57	0.33-0.64
Sara	Unknown	1986-2023	0.42-0.72	0.25-0.52	0.44-0.70	0.32-0.65

Table 6. Mean annual NDVI range for flaring sites at 240 m from the stack

Facility	Build time	Data dates	N (m)	E (m)	S (m)	W (m)
Eleme I	1965	1986-2023	0.50-0.62	0.85-0.86	0.77-0.80	0.48-0.54
Eleme II	1988	1984-2023	0.60-0.70	0.65-0.71	0.60-0.64	0.45-0.54
Onne	2010	1984-2023	0.45-0.53	0.62-0.64	0.60-0.70	0.65-0.69
Umurolu	Unknown	1984-2023	0.50-0.58	0.48-0.56	0.75-0.78	0.50-0.59
Bonny	1989	1986-2023	0.55-0.59	0.50-0.53	0.48-0.52	0.51-0.53
Alua	Unknown	1984-2023	0.45-0.53	0.61-0.64	0.60-0.65	0.69-0.70
Rukpokwu	Unknown	1986-2023	0.75-0.79	0.74-0.81	0.48-0.59	0.51-0.53
Obigbo	Unknown	1986-2023	0.45-0.52	0.65-0.69	0.65-0.67	0.81-0.84
Chokocho	Unknown	1986-2023	0.75-0.79	0.73-0.74	0.52-0.61	0.42-0.50
Umudioga	Unknown	1984-2023	0.75-0.78	0.66-0.69	0.61-0.69	0.42-0.50
Sara	Unknown	1986-2023	0.50-0.60	0.48-0.54	0.75-0.78	0.50-0.61

Table 7. Mean NDVI for Eleme I at (60, 90, 120 and 240) m from the stack

Facility	Build time	Data dates	N (m)	E (m)	S (m)	W (m)
Eleme I (60 m)	1965	1986-2023	0.445	0.555	0.529	0.490
Eleme I (90 m)		1986-2023	0.470	0.600	0.655	0.510
Eleme I (120 m)		1986-2023	0.605	0.685	0.685	0.610
Eleme I (240 m)		1986-2023	0.660	0.855	0.785	0.645

Table 8. Mean NDVI for Eleme II at (60, 90, 120 and 240) m from the stack

Facility	Build time	Data dates	N (m)	E (m)	S (m)	W (m)
Eleme II (60 m)	1988	1984-2023	0.485	0.485	0.485	0.445
Eleme II (90 m)		1984-2023	0.485	0.505	0.550	0.450
Eleme II (120 m)		1984-2023	0.555	0.540	0.490	0.485
Eleme II (240 m)		1984-2023	0.650	0.680	0.620	0.495

Table 9. Mean NDVI for Onne at (60, 90, 120 and 240) m from the stack

Facility	Build time	Data dates	N (m)	E (m)	S (m)	W (m)
Onne (60 m)	2010	1984-2023	0.490	0.630	0.515	0.520
Onne (90 m)		1984-2023	0.570	0.515	0.550	0.590
Onne (120 m)		1984-2023	0.605	0.650	0.570	0.610
Onne (240 m)		1984-2023	0.670	0.685	0.650	0.670

Table 10. Mean NDVI for Umurolu at (60, 90, 120 and 240) m from the stack

Facility	Build time	Data dates	N (m)	E (m)	S (m)	W (m)
Umurolu (60 m)	Unknown	1984-2023	0.525	0.405	0.590	0.510
Umurolu (90 m)		1984-2023	0.540	0.405	0.595	0.545
Umurolu (120 m)		1984-2023	0.560	0.565	0.765	0.565
Umurolu (240 m)		1984-2023	0.590	0.855	0.785	0.695

Table 11. Mean NDVI for Bonny at (60, 90, 120 and 240) m from the stack

Facility	Build time	Data dates	N (m)	E (m)	S (m)	W (m)
Bonny (60 m)	1989	1986-2023	0.455	0.455	0.445	0.380
Bonny (90 m)		1986-2023	0.445	0.445	0.450	0.475
Bonny (120 m)		1986-2023	0.540	0.515	0.468	0.494
Bonny (240 m)		1986-2023	0.570	0.590	0.500	0.520

Table 12. Mean NDVI for Alua at (60, 90, 120 and 240) m from the stack

Facility	Build time	Data dates	N (m)	E (m)	S (m)	W (m)
Alua (60 m)	Unknown	1984-2023	0.460	0.480	0.600	0.515
Alua (90 m)		1984-2023	0.460	0.495	0.455	0.512
Alua (120 m)		1984-2023	0.480	0.515	0.455	0.610
Alua (240 m)		1984-2023	0.500	0.625	0.625	0.695

Table 13. Mean NDVI for Rukpokwu at (60, 90, 120 and 240) m from the stack

Facility	Build time	Data dates	N (m)	E (m)	S (m)	W (m)
Rukpokwu (60 m)	Unknown	1986-2023	0.490	0.350	0.445	0.460
Rukpokwu (90 m)		1986-2023	0.530	0.490	0.485	0.500
Rukpokwu (120 m)		1986-2023	0.570	0.500	0.530	0.520
Rukpokwu (240 m)		1986-2023	0.770	0.775	0.535	0.5595

Table 14. Mean NDVI for Obigbo at (60, 90, 120 and 240) m from the stack

Facility	Build time	Data dates	N (m)	E (m)	S (m)	W (m)
Obigbo (60 m)	Unknown	1986-2023	0.380	0.300	0.485	0.475
Obigbo (90 m)		1986-2023	0.445	0.480	0.515	0.490
Obigbo (120 m)		1986-2023	0.485	0.500	0.606	0.500
Obigbo (240 m)		1986-2023	0.530	0.670	0.660	0.825

Table 15. Mean NDVI for Chokocho at (60, 90, 120 and 240) m from the stack

Facility	Build time	Data dates	N (m)	E (m)	S (m)	W (m)
Chokocho (60 m)	Unknown	1986-2023	0.480	0.350	0.485	0.460
Chokocho (90 m)		1986-2023	0.500	0.500	0.565	0.463
Chokocho (120 m)		1986-2023	0.570	0.560	0.615	0.575
Chokocho (240 m)		1986-2023	0.770	0.735	0.640	0.615

Table 16. Mean NDVI for Umudioga at (60, 90, 120 and 240) m from the stack

Facility	Build time	Data dates	N (m)	E (m)	S (m)	W (m)
Umudioga (60 m)	Unknown	1984-2023	0.570	0.290	0.445	0.460
Umudioga (90 m)		1984-2023	0.590	0.600	0.505	0.475
Umudioga (120 m)		1984-2023	0.625	0.610	0.510	0.480
Umudioga (240 m)		1984-2023	0.765	0.675	0.650	0.485

Table 17. Mean NDVI for Sara at (60, 90, 120 and 240) m from the flare stack

Facility	Build time	Data dates	N (m)	E (m)	S (m)	W (m)
Sara (60 m)	Unknown	1986-2023	0.550	0.385	0.550	0.485
Sara (90 m)		1986-2023	0.580	0.480	0.570	0.495
Sara (120 m)		1986-2023	0.612	0.500	0.575	0.555
Sara (240 m)		1986-2023	0.655	0.510	0.765	0.590

At Eleme Refinery I (Figure 3), NDVI at 60 m from the flare in the 4 directions shows slow and stable decrease in values until 2001 when there was a gradual reduction in its values. At 60 m from the flare in the W direction, the NDVI value reduced from 0.42 m in 2022 to 0.24 m in 2023. Figure 4 presents NDVI for Eleme Refinery II which gives a yearly reduction of its values. However, at 240 m NDVI values were almost sustained from 1984 to 2008; and from 2008 to 2023 values of NDVI increase slowly. This is due to the damage of the Refinery II since 2008 that led to reduction in the production capacity to about 10 %. From Figure 5 (Onne), there were no changes in the value of NDVI (1984-2008). However, at 60 and 90 m for the 4 directions from 2008 and 2015 NDVI fluctuated. In 2008, at 120 m, NDVI reduced from 0.62 m to (0.52-0.48) m in 2009. Furthermore, Umurolu (Figure 6) show slow increase in the NDVI values (0.50-0.59) m from 1984 to 2023 with the maximum value recorded in 2009.

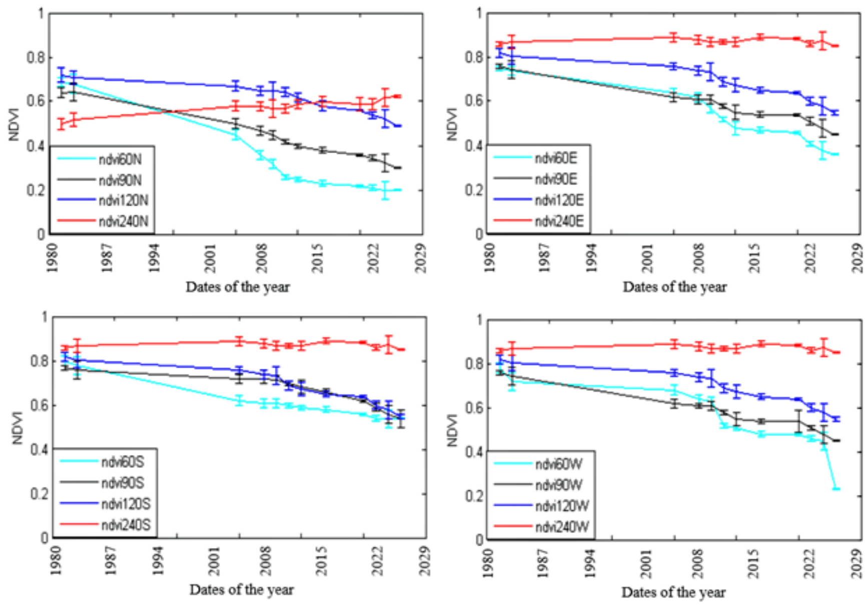

Figure 3. NDVI value changes over time in Eleme refinery I (1986-2023)

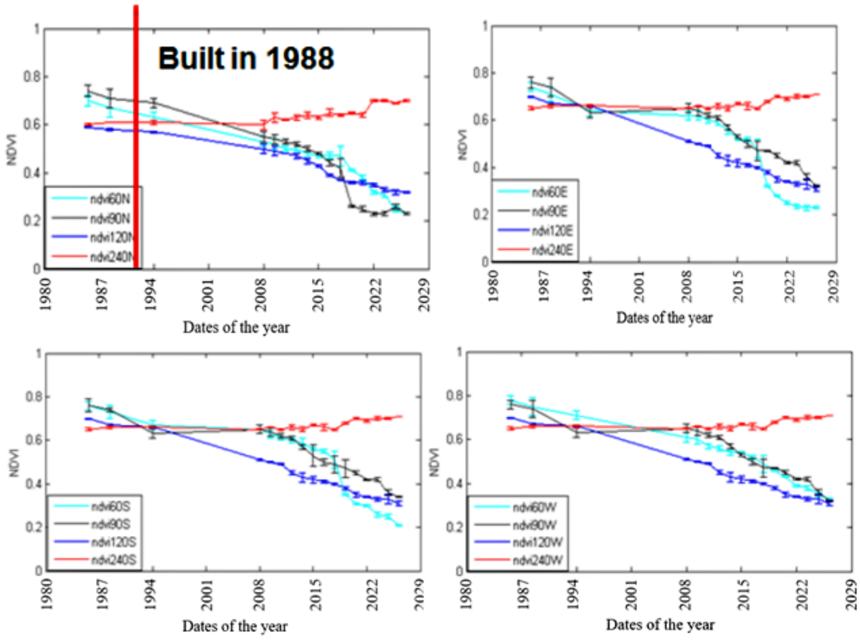

Figure 4. NDVI value changes over time in Eleme refinery II (1984-2023)

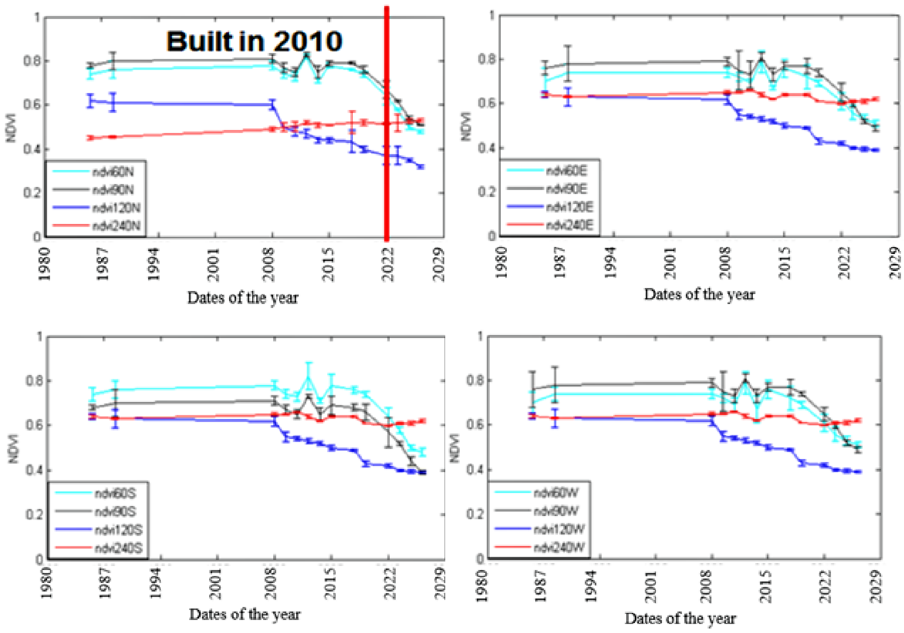

Figure 5. NDVI value changes over time in Onne (1984-2023)

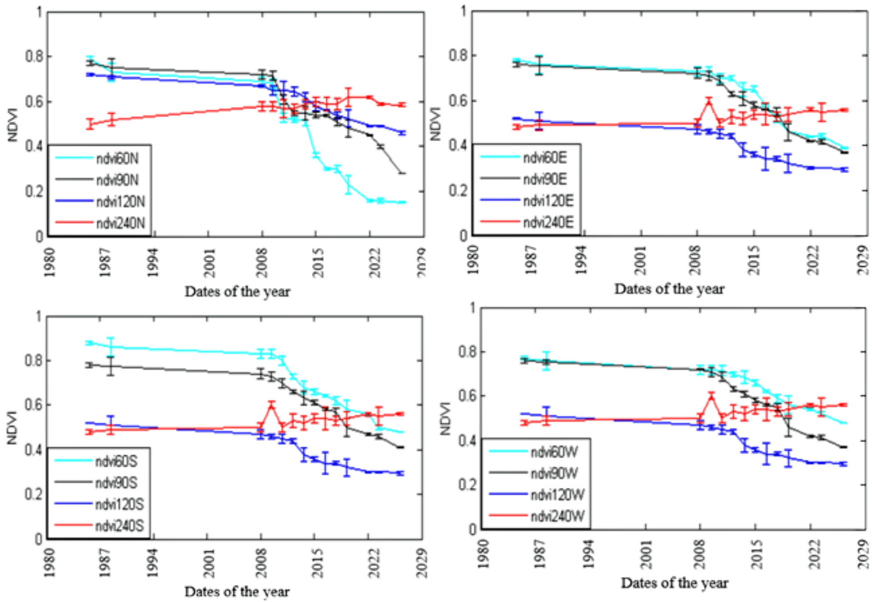

Figure 6. NDVI value changes over time in Umurolu (1984-2023)

From (2008-2023) NDVI reduced at 60 m N for Bonny LNG (Figure 7) but at 90 m there was a great reduction in 2006. At 120 m NDVI values were almost constant (1986-2004), and from here the NDVI steadily reduced until 2023. However, at 240 m NDVI values increased from (0.5) m in 2001 to 0.55 m and above in 2023. General annual reductions of NDVI were recorded for Alua (Figure 8), Rukpokwu (Figure 9), Obigbo (Figure 10), Chokocho (Figure 11), Umudioga (Figure 12) and Sara (Figure 13) in the N, E, S, and W directions. However, for Alua, at 240 m NDVI slowly increased for all directions. For Obigbo, at a distance of 240 m, the NDVI gave the same values for all directions. For Umudioga N, NDVI reduced from 2008 to 2023 (0.5-0.7). For Sara at 240 m NDVI increased from 1990 to 2002 (0.48-0.71), reduced in 2005 (0.58) and then slowly increased until 2023. The lowest mean NDVI (0.290) obtained from all the 11 sites is recorded at Umudioga 60 m E of the flare stack, followed by Obigbo with (0.300) at 60 m East of the flare. Finally, both Rukpokwu and Chokocho recorded (0.350) at 60 m East of the stack.

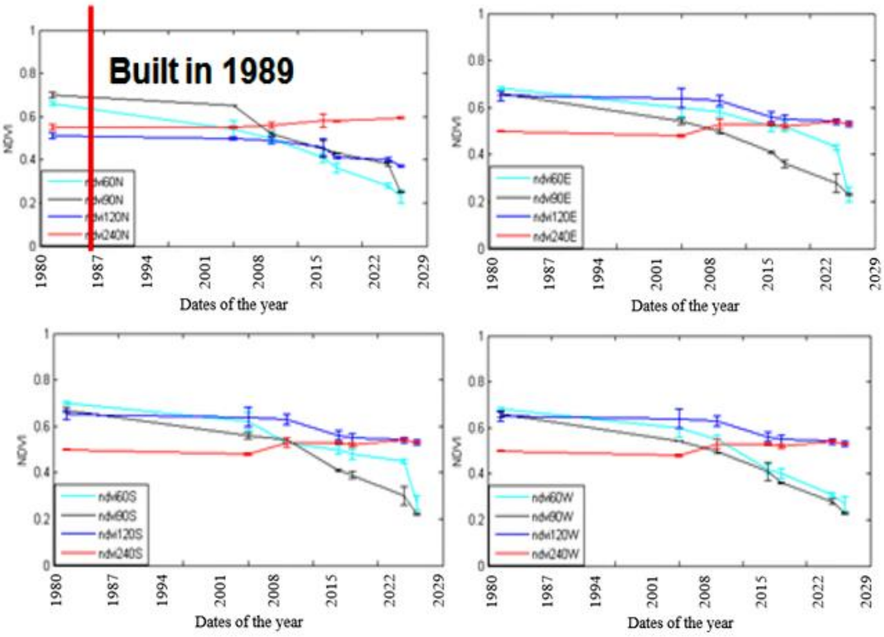

Figure7. NDVI value changes over time in Bonny LNG (1986-2023)

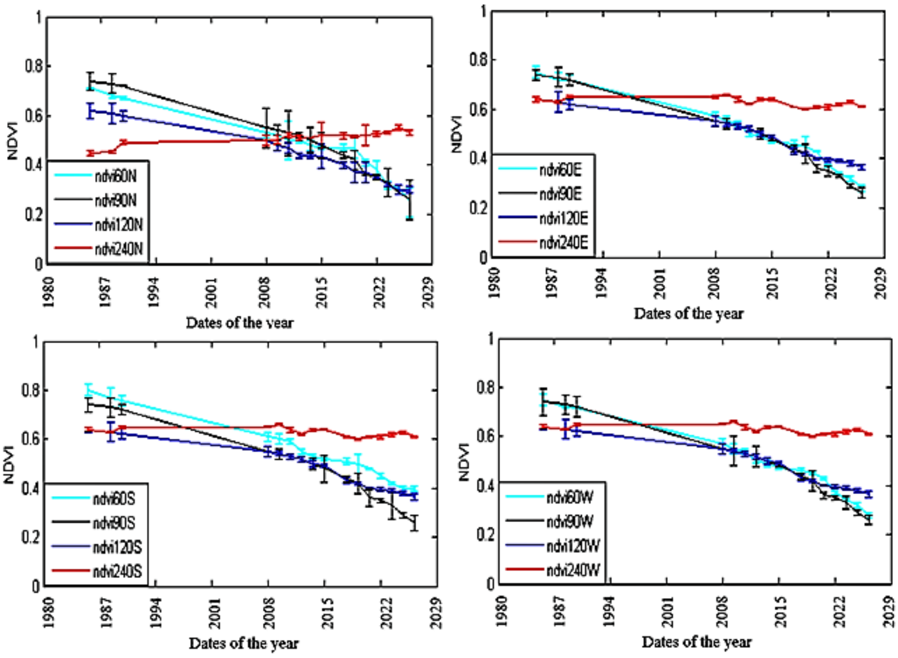

Figure 8. NDVI value changes over time in Alua (1984-2023)

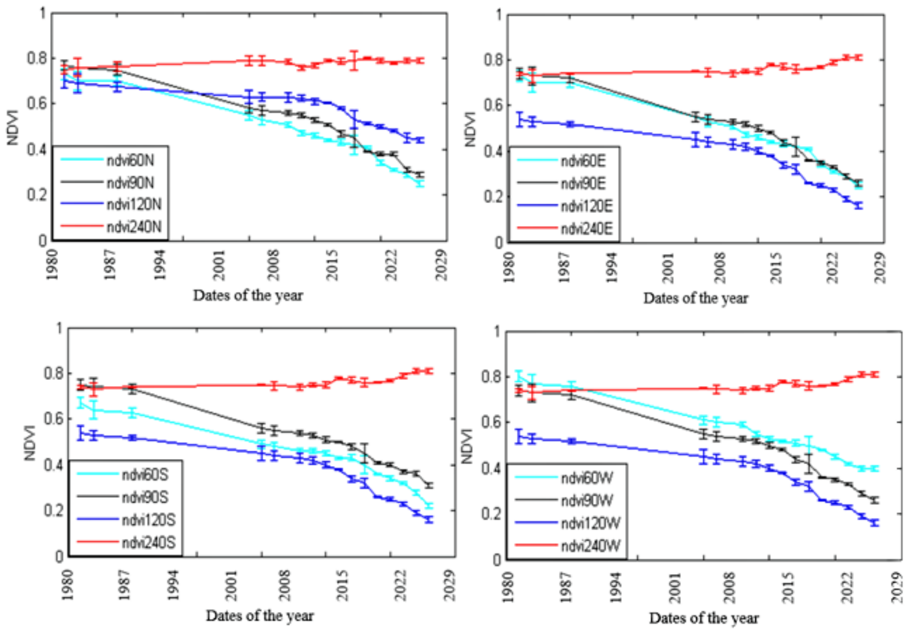

Figure 9. NDVI value changes over time in Rukpokwu (1986-2023)

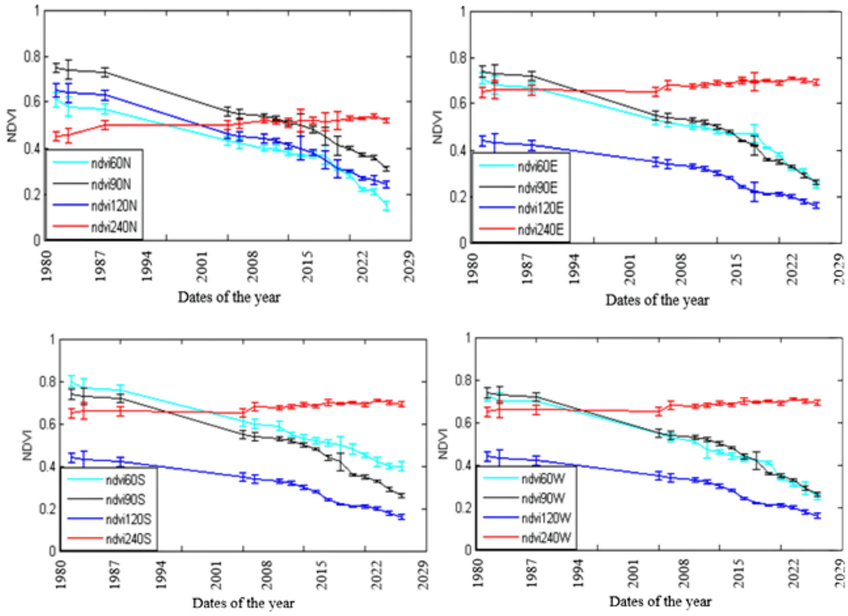

Figure 10. NDVI value changes over time in Obigbo (1986-2023)

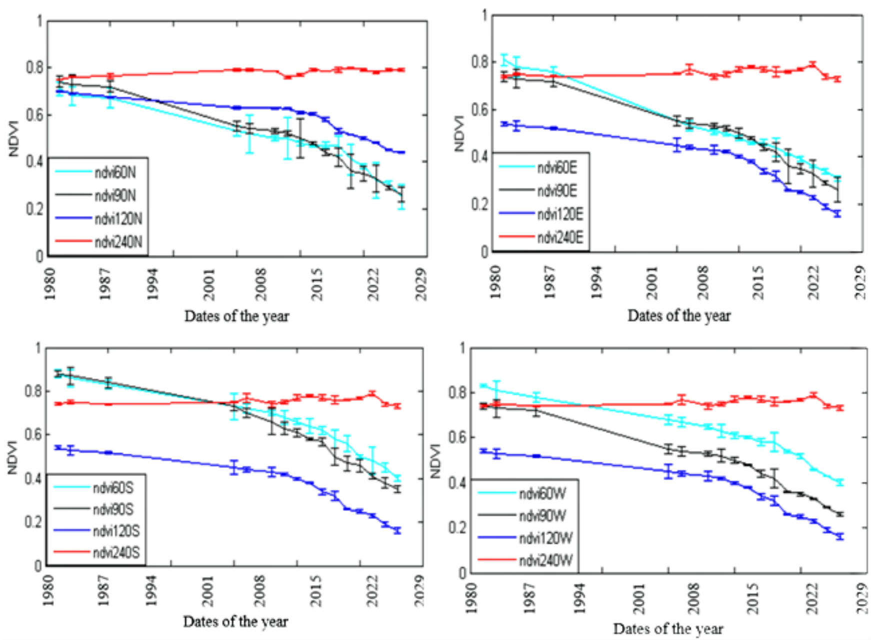

Figure 11. NDVI value changes over time in Chokocho (1986-2023)

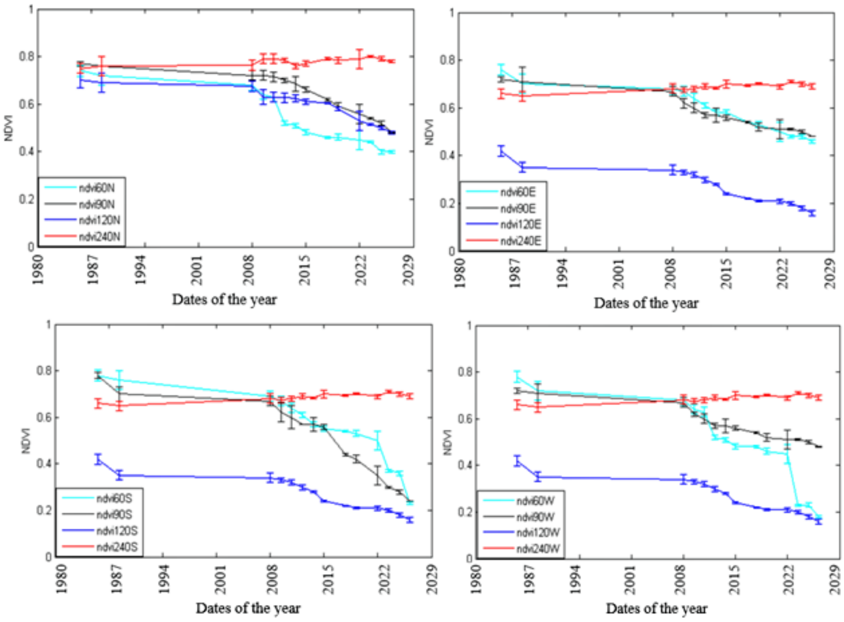

Figure 12. NDVI value changes over time in Umudioga (1984-2023)

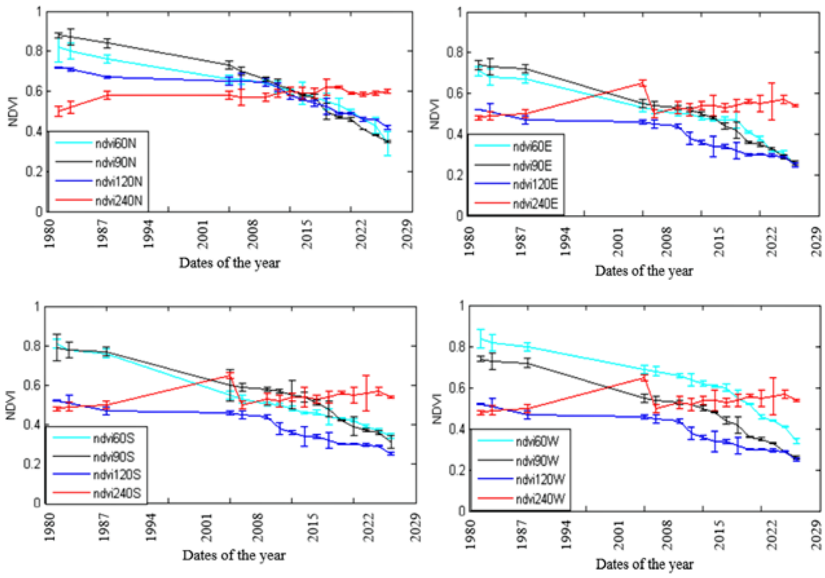

Figure 13. NDVI value changes over time in Sara (1986-2023)

3.2. Statistical analysis

The NDVI results for each pixel in each subscene from 1984 to 2023 were linearly regressed against time. The mean and standard deviation of NDVI trend values were calculated in each case for NDVI trend values. The significance level adopted for the analysis is α >0.05. Table 18 presents the mean and standard deviation (SD) for all the NDVI values at each flaring site. Column 1 gives the list of the 11 flaring sites studied, columns 2 and 3 shows the computed mean and standard deviation of NDVI recorded for all pixels within 12 × 12 km of each site.

Table 18. Mean and SD for NDVI values for the study sites (Change in NDVI/ year)

Flaring sites	Mean (All pixels)	SD (All pixels)
Eleme I	1.9166×10^{-5}	2.0689×10^{-4}
Eleme II	1.5010×10^{-5}	1.3596×10^{-4}
Onne	2.2849×10^{-6}	7.9515×10^{-5}
Umurolu	5.8057×10^{-5}	7.4988×10^{-5}
Bonny	2.1294×10^{-5}	8.2903×10^{-5}
Alua	8.7469×10^{-5}	1.4516×10^{-4}
Rukpokwu	7.3986×10^{-5}	6.2093×10^{-5}
Obigbo	7.8273×10^{-5}	1.1192×10^{-4}
Chokocho	1.0520×10^{-4}	5.0786×10^{-5}
Umudioga	-3.0408×10^{-5}	1.0120×10^{-4}
Sara	1.4015×10^{-5}	7.6382×10^{-5}

Mean gives a central value in the distribution; however, it does not indicate how far the data points fall from the center. SD value summarizes the variability in a dataset; and also represents the typical distance between each data point and the mean. A smaller value of SD shows that the data points cluster closer to the mean which is an indication that the values in the dataset are relatively consistent. In contrast, higher values show that the values spread out further from the mean. The results presented in Table 18 show that SD for each site is small with a range value (5.0786×10^{-5} - 2.0689×10^{-4}). Chokocho site recorded the lowest SD (5.0786×10^{-5}) and the highest value is for Eleme refinery 1. The NDVI results obtained for all sites are directly opposite to the temperature which is supported by the previous literature [1, 5, 9, 14]. The higher the temperature around the flare source, the lower NDVI retrieved. Hence, contamination of vegetation, destruction of farm produce, stunted growth and/or death of vegetation and agricultural products, environmental pollution etc. at each site is inevitable.

4. Discussion

The lowest values of NDVI were obtained at 60 m and the values increase as distance from the flare increases to 90 m, 120 and 240 m for all the 11 sites throughout the years of analysis. However, before the construction of Onne (1984-2008) NDVI fluctuated which could be attributed to the vegetation density, vegetation types and their photosynthetic rate as no flare was present. The results also recorded yearly reduction in NDVI within 120 m from the stack; and that the impacts of the flare after 120 m are very little. Also, the results from the statistical analysis give smaller SD which means that the data cluster to the mean i.e. the dataset values is consistent. The implication of the results is that vegetation closer to the flare is sparse, unhealthy and some of it is dead. The lowest mean NDVI (0.290) obtained from all the 11 sites is recorded at Umudioga 60 m E of the flare stack. Therefore, it can be concluded that Landsat sensors can be used to evaluate the changes in vegetation cover and its health at the flaring sites in the Niger Delta.

Lack of data on vegetation types, and the rate and volume of the gas burning at flaring sites are two major challenges to this research. Therefore, a further study needs to be carried out using these two datasets in order to improve on the results obtained for this study.

Gas flaring is a major problem in Nigeria that has not yet received 100 % attention of the Government on how to solve it. Hence, the following recommendations are made:

- Nigerian Government should carry out the **s**tringent enforcement of the Nigerian Petroleum Industry Act of 2021.

- Nigerian Environmental protection laws should have adequate provisions for combating oil and gas pollution, degradation, and gas flaring. The National Environmental Standard Regulation Enforcement Agency (Establishment) Act (NESREA), 2007, should be amended to widen its scope to oil and gas sector activities.
- The Nigerian Constitution should be amended to make environmental infringements justiciable in order to guarantee a healthy and sustainable environment.
- Enactment of the comprehensive regulatory framework governing gas utilization and development of gas pipeline networks to all the six (6) geo-political zones in Nigeria for proper gas distribution.
- The Nigerian Government should increase generation of electricity in Nigeria through the use of gas.
- Oil companies should update their equipment to modern technologies and methods to be in accordance with the international standards.
- Nigerian Government should encourage investors in the energy sector by providing the enabling environment.
- A gas flaring price targeting natural gas companies should be more effective in mitigating gas flaring than the wider ‘carbon price’ or pollution price/tax policy.
- The Federal Government should provide alternative energy source to mitigate the effect of gas flaring on the people and preserve the environment.

Acknowledgements

The Author is grateful to the USGS for the provision of Landsat data and ATMCORR Calculator. Many thanks to Jill Schwarz for MATLAB coding and guidance.

Conflict of Interest

The Author declares no conflict of interest.

Author Contribution

B. M. performed the research and analysis and wrote the whole manuscript.

References

[1] Lu, W., Liu, Y., Wang, J., Xu, W., Wu, W., Liu, Y., Zhao, B., Li, H., & Pei Li. “Global proliferation of offshore gas flaring areas”. *Journal of Maps*, 16(2), 396-404, 2020. DOI: 10.1080/17445647.2020.1762773

[2] Morakinyo, B. O., Lavender, S., Schwarz, J & Abbott, V.. “Mapping of land cover and estimation of their emissivity values for gas flaring sites in the Niger Delta”. *British Journal of Environmental Sciences*, 7(2), 31-58, 2019.

[3] Morakinyo, B. O., Lavender, S & Abbott, V.. “Detection of potentially gas flaring related pollution on vegetation cover and its health using remotely sensed data in the Niger Delta, Nigeria”. *Asian Review of Environmental and Earth Sciences*, 10(1), 1-13, 2023a. https://doi.org/10.20448/arees.v10i1.4407

[4] Morakinyo, B. O.. “Assessments of the impacts of environmental factors on vegetation cover at gas flaring sites in the Niger Delta, Nigeria”. *Review of Environment and Earth Sciences*, 10(1), 8-18, 2023b.

[5] Umbugala, U. D & Morakinyo, B. O.. “Detection of Oil and Gas Platforms in the Niger Delta, Nigeria: Role of Digital Technology in Facilities Management”. *BAZE University Journal of Entrepreneurship and Interdisciplinary Studies,* 2(2), 11-22, 2023.

[6] Morakinyo, B. O.. “Flaring and pollution detection in the Niger Delta using remote sensing”. PhD Thesis, University of Plymouth, Plymouth, United Kingdom. 2015.

[7] Morakinyo, B. O., Lavender, S &Abbott, V.. “Investigation of potential prevailing wind impact on land surface temperature at gas flaring sites in the Niger Delta, Nigeria”. *International Journal of Environment and Geoinformatics,* 9(1), 179-190, 2022a. https://doi.org/10.30897/ijegeo.968687

[8] Morakinyo, B. O., Lavender, S & Abbott, V.. “Evaluation of factors influencing changes in land surface temperature at gas flaring sites in the Niger Delta, Nigeria”. *BAZE University Journal of Entrepreneurship and Interdisciplinary Studies,* 1(2), 1-19, 2022b.

[9] Nwaogu, L. A & Onyeze, G. O. C.. “Environmental Impacts of Gas Flaring on Ebocha-Egbema, Niger Delta, Nigeria”. *Energy and Environmental Research,* 8(1), 1-11, 2020.

[10] Morakinyo, B. O.. “Detection of Impacts of Gas Flaring in the Environment: Application of Landsat Earth Observation Data”. *BAZE University Journal of Entrepreneurship and Interdisciplinary Studies,* 2(1), 74-89, 2023c.

[11] Morakinyo, B. O., Lavender, S & Abbott, V.. “The methodology and results from ground validation of satellite observations at gas Flaring Sites in Nigeria”. *International Journal of Environment and Geoinformatics,* 8(3), 290-300, 2021. https://doi.org/10.30897/ijegeo.749664

[12] Morakinyo, B. O., Lavender, S & Abbott, V.. “Assessment of uncertainties in the computation of atmospheric correction parameters for Landsat 5 TM and Landsat 7 ETM+ thermal band from atmospheric correction parameter (ATMCORR calculator)”. *British Journal of Environmental Sciences,* 8(1), 20-30, 2020a.

[13] Morakinyo, B. O., Lavender, S & Abbott, V.. “Retrieval of land surface temperature from Earth observation satellites for gas flaring sites in the Niger Delta, Nigeria”. *International Journal of Environmental Monitoring and Analysis.* 8(3), 59-74, 2020b. https://doi.org/10.11648/j.ijema.20200803.13

[14] Musa, D. G., Oruonye, E. D., Anger, R. T., Ojeh, V. N & Delphine, D.. “Effect of Gas Flaring on Human Well-Being and Environment in Obodo-Ugwa, Ndokwa West, Local Government Area, Delta State, Nigeria”. *Journal of Engineering & Environmental Science 2024, 2(1): 000108),* 2024.

[15] Huang, S., Tang, L., Hupy, P., Wang, Y & Shao, G.. “A commentary review on the use of normalized difference vegetation index (NDVI) in the era of popular remote sensing”. *Journal of Forestry Research* 32(1), 1-6, 2020. https://doi.org/10.1007/s11676-020-01155-1

[16] Kalisa, W., Igbawua, T., Henchiri, M., Ali, S., Zhang, S., Bai, Y & Zhang, J.. “Assessment of climate impact on vegetation dynamics over East Africa from 1982 to 2015”. *Scientific Reports,*9:16865, 2019. https://doi.org/10.1038/s41598-019-53150-0

[17] Hua, X., Rena, H., Tansey, K., Zhenga, Y., Ghent, D., Liu, X & Yan, L.. “Agricultural drought monitoring using European Space Agency Sentinel 3A land surface temperature and normalized difference vegetation index imageries”. *Agricultural and Forest Meteorology*, 279, 107707, 2019.

[18] Wei., W., Zhang, H., Zhou, J., Zhou, L., Xie, B. & Li, C. "Drought monitoring in arid and semi-arid region based on multi-satellite datasets in Northwest China". *Environmental Science and Pollution Research*, vol. 28, pages 51556-51574, 2021.

19] Karnieli, A., Agam, N., Pinker, R. T., Anderson, M., Imhoff, M. L., Gutman, G. G., Panov, N & Goldberg, A.. "Use of NDVI and Land Surface Temperature for Drought Assessment: Merits and Limitations". *Journal of Climate*, 23: 618-633, 2010.

[20] Polat, A. B., Akcay, O & Kontas, F.. "Drought monitoring in Burdur Lake, Turkey using multi-sensor remote sensing data sets". *Advances in Geodesy and Geoinformation (formerly Geodesy and Cartography)*, Vol. 73, no. 1, article no. e47, 2024. https://doi.org/10.24425/agg.2023.146159

[21] Gessner, U.; Reinermann, S., Asam, S & Kuenzer, C. "Vegetation Stress Monitor-Assessment of Drought and Temperature-Related Effects on Vegetation in Germany Analyzing MODIS Time Series over 23 Years". Remote Sensing, 15, 5428, 2023. https://doi.org/10.3390/rs15225428

[22] Kloos, S., Yuan, Y., Castelli, M & Menzel, A.. "Agricultural Drought Detection with MODIS Based Vegetation Health Indices in Southeast Germany". Remote Sensing, 13, 3907, 2021. https://doi.org/10.3390/rs13193907

[23] Chang, J., Liu, Q., Wang, S & Huang, C. "Vegetation Dynamics and Their Influencing Factors in China from 1998 to 2019". Remote Sensing, 14, 3390, 2022. https://doi.org/10.3390/rs14143390

[24] Chrysopolitou, V., Apostolakis, A., Avtzis, D., Avtzis, N., Diamandis, S., Kemitzoglou, D., Papadimos, D., Perlerou, C., Tsiaoussi, V & Dafis, S.. "Studies on forest health and vegetation changes in Greece under the effects of climate changes". Biodiversity Conservation, 22:1133-1150, 2013. DOI 10.1007/s10531-013-0451-2.

[25] Lavender, S. J.. "Monitoring land cover dynamics at varying spatial scales using high to very high resolution optical imagery". *The International Archives of the Photogrammetry, Remote Sensing and Spatial Information Sciences*, Volume XLI-B8, XXIII ISPRS Congress, 12-19 July 2016, Prague, Czech Republic.

[26] Jiang, L., Liu, Y., Wu, S & Yang, C.. "Analyzing ecological environment change and associated driving factors in China based on NDVI time series data". *Ecological Indicators*, 129, 107933, 2021.

[27] Hu, Y., Raza, A., Syed, N. R., Acharki, S., Ray, R. L., Hussain, S., Dehghanisanij, H., Zubair, M & Elbeltagi, A.. "Land Use/Land Cover Change Detection and NDVI Estimation in Pakistan's Southern Punjab Province". *Sustainability*, 15, 3572, 2023. https://doi.org/10.3390/su15043572

[28] Guha, S.. "A long-term monthly assessment of land surface temperature and normalized difference vegetation index using Landsat data". *urbe. Revista Brasileira de Gestão Urbana*, v.13, e20200345, 2021. https://doi.org/10.1590/2175-3369.013.e20200345

[29] Guha, S., Govil, H & Diwan, P.. "Monitoring LST-NDVI Relationship Using Premonsoon Landsat Datasets". *Advances in Meteorology*, Volume 2020, Article ID 4539684, 15 pages, 2020. https://doi.org/10.1155/2020/4539684

[30] Roßberg, T & Schmitt, M.. "A Globally Applicable Method for NDVI Estimation from Sentinel-1 SAR Backscatter Using a Deep Neural Network and the SEN12TP Dataset". PFG, 91: 171-188, 2023.

[31] Pettorelli, N., Vik, J. O., Mysterud, A., Gaillard, J. M., Tucker, C. J & Stenseth, N. C.. "Using the satellite-derived NDVI to assess ecological responses to environmental change". *Trends of Ecological Evolution,* 20(9), 503-510, 2005.

[32] Tian, J., Wang, L., Li, X., Gong, H., Shi, C., Zhong, R & Liu, X.. "Comparison of UAV and WorldView-2 imagery for mapping leaf area index of mangrove forest". *International Journal of Applied Earth Observation and Geoinformatics,* 61, 22-31, 2017.

[33] Pastor-Guzman, J., Atkinson, P., Dash, J & Rioja-Nieto, R.. "Spatio-temporal variation in mangrove chlorophyll concentration using Landsat 8". *Remote Sensing of Environment,* 7(11), 14530-14558, 2015.

[34] Vicente-Serrano, S. M., Camarero, J. J., Olano, J. M., Martín-Hernández, N., Peña-Gallardo, M., Tomás-Burguera, M., Gazol, A., Azorin-Molina, C., Bhuyan, U & El-Kenawy, A.. "Diverse relationships between forest growth and the normalized difference vegetation index at a global scale". *Remote Sensing of Environment,* 187, 14-29, 2016.

[35] Chavez, R. O., Clevers, J. G. P. W., Decuyper, M., De Bruin, S & Herold, M.. "50 years of water extraction in the Pampa del Tamarugal basin: Can Prosopis tamarugo trees survive in the hyper-arid Atacama Desert (Northern Chile)?". *Journal of Arid Environment,* 124, 292-303, 2016.

[36] Butt, B.. "Environmental indicators and governance". *Current Opinion on Environmental Sustainability* 32, 84-89, 2018.

[37] Grant, B. G.. "UAV imagery analysis: Challenges and opportunities. In: Proceedings of the long-range imaging II". Anaheim, CA, vol 10204, p 1020406, 2017.

[38] Jones, H. G & Vaughan, R. A.. "Remote sensing of vegetation: Principles, techniques and applications". Oxford University Press, New York, p 353, 2010.

[39] Chu, H. S., Venevsky, S., Wu, C & Wang, M. H.. "NDVI-based vegetation dynamics and its response to climate changes at Amur-Heilongjiang River Basin from 1982 to 2015". *Sci. Total Environ*. 650, 2051-2062, 2019. https://doi.org/10.1016/j. scitotenv.2018.09.115

[40] Mao, D., Wang, Z., Luo, L & Ren, C.. "Integrating AVHRR and MODIS data to monitor NDVI changes and their relationships with climatic parameters in Northeast China". *International Journal of Applied Earth Observation and Geoinformatics,* 18, 528-536, 2012. https://doi.org/10.1016/j. jag.2011.10.007

[41] Zhao, J., Huang, S., Huang, Q., Wang, H., Leng, G & Fang, W.. "Time-lagged response of vegetation dynamics to climatic and teleconnection factors". *Catena,* 189, 104474, 2020. https://doi.org/10.1016/j.catena.104474

[42] Buyantuyev, A & Wu, J.. "Urbanization diversifies land surface phenology in arid environments: Interactions among vegetation, climatic variation, and land use pattern in the Phoenix metropolitan region, USA". *Landscape Urban Plan,* 105 (1-2), 149-159, 2012. https://doi.org/10.1016/j.landurbplan.2011.12.013

[43] Olujobi, O. J.. "Analysis of the Legal Framework Governing Gas Flaring in Nigeria's Upstream Petroleum Sector and the Need for Overhauling". *Social Science,*9, 132, 2020.

[44] Aigbe, G. O., Cotton, M & Stringer, L. C.. "Global gas flaring and energy justice: An empirical ethics analysis of stakeholder perspectives". *Energy Research & Social Science* 99, 103064, 2023.

[45] Olujobi, O. J., Yebisi, T. E., Patrick, O. P & Ariremako, A. I.. "The Legal Framework for

Combating Gas Flaring in Nigeria's Oil and Gas Industry: Can It Promote Sustainable Energy Security?". *Sustainability*, 14, 7626, 2022. https://doi.org/10.3390/su1413762.

[46] Alola, A. A., Onifade, S. T., Magazzino, C & Obekpa, H. O.. "The effects of gas flaring as moderated by government quality in leading natural gas flaring economies". *Scientific Reports*,13: 14394, 2023. https://doi.org/10.1038/s41598-023-38032-w.

[47] Sandunika, D.M.I., Dilka, S.H.S., Alwis, M.K.S.D., Siriwardhana, S.M.G.T., M. S, N., Perera, W.A.V.T., Sandeepa, R.A.H.T., Panagoda, L.P.S.S., Chamara, N.N., & Kumarasiri, K.A.C.S.. "Assessing the effectiveness and sustainability of carbon capture and storage (ccs) technologies for mitigating greenhouse gas emissions". 2020.

[48] Thepsaskul, W., Wongsapai, W., Sirisrisakulchai, J., Jaitiang, T., Daroon, S., Raksakulkan, V., Muangjai, P., Ritkrerkkrai, C., Suttakul, P., & Wattakawigran, G.. "Potential business models of carbon capture and storage (CCS) for the oil refining industry in Thailand". *Energies*, *16*(19), p.6955, 2023.

[49] Ekemezie, I. O & Digitemie, W. N,. "Climate change mitigation strategies in the oil and gas sector. A review of practices and impact". *Engineering Science & Technology Journal*, Volume 5, Issue 3, 935-948, 2024.

[50] Van Oort, E., Chen, D., Ashok, P., & Fallah, A.. "Constructing deep closed-loop geothermal wells for globally scalable energy production by leveraging oil and gas ERD and HPHT well construction expertise". In SPE/IADC Drilling Conference and Exhibition (p. D021S002R001). SPE. 2021, March.

[51] Lyons, W. C., Stanley, J. H., Sinisterra, F. J., & Weller, T.. "Air and Gas Drilling Manual: Applications for Oil, Gas, Geothermal Fluid Recovery Wells, Specialized Construction Boreholes, and the History and Advent of the Directional DTH". *Gulf Professional Publishing*. 2020.

[52] Elvidge, C. D., Bazilian, M. D., Zhizhin, M., Ghosh, T., Baugh, K & Hsu, F. (2018). The potential role of natural gas flaring in meeting greenhouse gas mitigation targets. Energy Strategy Reviews 20 (2018) 156-162.

[53] Zolfaghari, M., Pirouzfar, V and Sakhaeinia, H.. "Technical characterization and economic evaluation of recovery of flare gas in various gas-processing plants". *Energy* 124481-491, 2017.

[54] ESRI.. "Map of Nigeria, map of Rivers State and map of 11 gas flaring studied sites". 2024.

[55] Chander, G & Markham, K.. "Revised Landsat 5 TM Radiometric Calibration Procedures and Post Calibration Ranges". *IEEE Transaction of Geosciences and Remote Sensing* 41(11): 2674-2677, 2003.

[56] NASA.. "National Aeronautics and Space Administration. Landsat 7 ETM+ Science Data Users Handbook". [Online]. Available: http://www.landsathandbook.gsfc.nasa.gov/data_prod/prog_sect11_3.html [Accessed 23rd January 2022].

[57] Ihlen, V.. "Landsat 8 (L8) Data Users Handbook", Version 5.0. Department of the Interior, U.S. Geological Survey. 2019.

[58] Markham, B. L &Barker, J. L.. "Landsat MSS and TM post-calibration dynamic ranges, exoatmospheric reflectances and at-satellite temperature". *EOSAT Landsat Technical Notes*: 3-8, 1986.

[59] Lavender, S. J.. "Monitoring land cover dynamics at varying spatial scales using high to very high resolution optical imagery". *The International Archives of the Photogrammetry, Remote Sensing and Spatial Information Sciences*, Volume XLI-B8, XXIII ISPRS Congress, 12-19 July 2016, Prague, Czech Republic.

[60] Liang, S., Fang, H &Chen, M.. "Atmospheric Correction of Landsat ETM+ Land Surface Imagery - Part I: Methods". *IEEE Transactions on Geoscience and Remote Sensing* 39(11): 2490-2498, 2001.

[61] Chavez, P. S.. "Image-based Atmospheric Corrections-Revisited and Improved". *Photogrammetry Engineering and Remote Sensing* 62(9): 1025-1036, 1996.

[62] Santer, R., Carrere, V., Dubuisson, P & Roger, J. C.. "Atmospheric correction over land for MERIS". *International Journal of Remote Sensing* 20: 1819-1840, 1999.

[63] Şatır, O & Berberoğlu, S. (2012). Land Use/Cover Classification Techniques Using Optical Remotely Sensed Data in Landscape Planning, Landscape Planning, Dr. Murat Ozyavuz (Ed.), ISBN: 978-953-51-0654-8, InTech. [Online]. Available: http://www.intechopen.com/books/landscape-planning/land-use-cover-classificationtechniques-using-optical-remotely-sensed-data-in-landscape-plannin [Accessed 15th May 2023]

[64] Maaharjan, A.. "Land use/land cover of Katrimandu valley by using Remote Sensing and GIS. M.Sc. Dissertation submitted to Central Department of Environmental Sciences", Institute of Science and Technology, Tribhuvan University, Kirtipur, Kathmandu, Nepal. 2018.

[65] Huete, A., Didan, K., Miura, T., Rodriguez, E.P., Gao, X & Ferreira, L.G.. "Overview of the radiometric and biophysical performance of the MODIS vegetation indices". *Remote Sensing of Environment*, 83 (1-2), 195-213, 2002. https://doi.org/10.1016/S0034-4257(02) 00096-2

[66] Goward, S. N., Tucker, C. J. &Dye, D. G.. "North American vegetation patterns observed with the NOAA-7 Advanced Very High-Resolution Radiometer". *Vegetation*, 64, 3-14, 1985.